Microporous and Mesoporous Materials 172 (2013) 95–104

Contents lists available at SciVerse ScienceDirect

Microporous and Mesoporous Materials

journal homepage: www.elsevier.com/locate/micromeso

Investigation of NaY Zeolite with adsorbed CO_2 by neutron powder diffraction

W. Wong-Ng [a,*], J.A. Kaduk [b], Q. Huang [c], L. Espinal [a], L. Li [d], J.W. Burress [e]

[a] Material Measurement Laboratory, National Institute of Standards and Technology, Gaithersburg, MD 20899, United States
[b] Department of Biological and Chemical Sciences, Illinois Institute of Technology, Chicago, IL 60616, United States
[c] NIST Center for Neutron Research, National Institute of Standards and Technology, Gaithersburg, MD 20899, United States
[d] Department of Materials Science and Engineering, Boise State University, Boise, ID 83725
[e] Physics and Astronomy Department, University of Missouri, Columbia, MO 65211, United States

ARTICLE INFO

Article history:
Received 25 November 2012
Received in revised form 16 January 2013
Accepted 19 January 2013
Available online 29 January 2013

Keywords:
Crystal structure of NaY zeolite with CO_2
Migration of the extra framework Na cations
Neutron diffraction
DFT calculations

ABSTRACT

The crystal structure of dehydrated NaY zeolite (Na-FAU structure type) with and without adsorbed CO_2 has been determined at 4 K and at room temperature (RT) using neutron powder diffraction techniques. The CO_2-containing sample was prepared at 195 K and 0.1 MPa p_{CO2} (dry ice sublimation conditions). Neutron diffraction data provides direct evidence that adsorption of CO_2 results in significant migration of the extraframework Na cations in the zeolite structure. At 4 K, 45 of the apparent 76 CO_2/cell were located in two crystallographically independent sites bonding to the Na cations (Na10) in the supercage site II. While the CO_2 molecule in the first site has a linear configuration interacting with Na10 via one terminal oxygen, the CO_2 molecule in the second site appears to have a bent O–C–O configuration (148.3(3)°), with both oxygen atoms coordinating to two symmetry-related Na10. Using DFT total energy calculations we found that the Na–CO_2 interaction slightly facilitates the bending motion for CO_2 by decreasing the energy cost for the 148.3(3)° bond angle by ≈0.2 eV/CO_2. However, this Na–CO_2 interaction is not enough to cause a 32° bond angle distortion in CO_2 (the energy cost of ≈0.66 eV/CO_2). We propose that rotational disorder plays a significant role in the appearance of the bent CO_2, while a small bending is possible. Our studies will help to provide a basis for interpreting CO_2 adsorption phenomena in NaY and related zeolites.

Published by Elsevier Inc.

1. Introduction

The relationship between increasing atmospheric CO_2 concentration and global warming is one of the most pressing environmental studies to date. To reduce the atmospheric level of CO_2 while minimizing the world economic impact, various carbon mitigation strategies are being developed. The implementation of carbon capture/sequestration policy in the coming years will need to be economically as well as environmentally attractive. Because existing coal-burning power plants are major contributors to CO_2 emissions (and it is expected that they will be a major part of energy production for the foreseeable future), reducing emissions from these plants is strategically important. Among the several approaches being considered to reduce emissions are: solvent absorption [1], adsorption in porous solid materials [2–11], chemical conversion [12], and deep sea deposition [13]. The research presented here is relevant to the goal of developing the technology of adsorption in porous solids as a technically feasible, affordable and energy-efficient solution.

Gas storage in porous solids is becoming an increasingly important technology with applications in energy-related, environmental, and biological areas [14]. Porous materials such as zeolites, polymers and metal-organic frameworks (MOFs) [2–8] offer a wide variety of compositions and structures that are suitable for adsorption and storage of various gases, including carbon dioxide. However, the challenge of developing materials with optimized CO_2 adsorption capacity remains, and a complete understanding of the adsorption mechanisms is still lacking. As a first step in addressing these issues, we have attempted to determine the detailed structural locations of adsorbed CO_2 molecules in an otherwise well-known zeolite host.

Zeolites are three-dimensional microporous crystalline solids with well-defined structures that contain aluminum, silicon, and oxygen in their regular framework. Various techniques to study the structures of zeolites have been reported, including X-ray diffraction, neutron diffraction [15] and solid state NMR [16]. The Si/Al atoms (T) are tetrahedrally coordinated with each other through shared oxygen atoms. Zeolites have cavities or channels that can host cations, water, or other molecules. Zeolites are promising materials for selective adsorption and separation of various absorbates including carbon dioxide. This class of materials provides an excellent basis for demonstrating how solid-state proper-

* Corresponding author. Tel.: +1 301 975 5791; fax: +1 975 5334.
E-mail address: Winnie.wong-ng@nist.gov (W. Wong-Ng).

1387-1811/$ - see front matter Published by Elsevier Inc.
http://dx.doi.org/10.1016/j.micromeso.2013.01.024

ties (such as pore size, pore architecture or chemical composition) can influence gas adsorption and diffusion processes. Diffusion of adsorbate molecules in zeolites plays an important role in several industrial applications related to separation and catalysis. Examples include: CO_2 post-combustion capture by indirect thermal swing adsorption [17], reduction in cost of CO_2 capture from flue gases [18], selective adsorption [19] and high-temperature adsorption of CO_2 [20], and mitigation of CO_2 contamination in oxygen production [21]. Theoretical treatments of the adsorption of CO_2 have been conducted for selected zeolites using the Monte Carlo simulation technique [22–24].

One particular zeolite, NaY (structure type FAU) [14,17–18,21–22,25–27], was chosen for the present study. Previous studies involving NaY include enhancement of the CO_2 retention capacity by Na- and Cs-treatments [27]. Molecular dynamics simulations using quasi-elastic neutron scattering experiments have also been carried out concerning CO_2 adsorption in NaY [28]. Although there are a number of studies concerning adsorption isotherms for CO_2 in NaY and theoretical prediction about the locations of the adsorbed CO_2, little experimental diffraction data is available concerning the location of the CO_2 molecules in the channels. The primary goals of this study are to determine the location of CO_2 molecules in the NaY-zeolite channels, the geometry of these molecules and the nature of their interactions with the zeolite framework and extraframework cations. In this paper, the structures of the dehydrated starting material (Na-FAU), and a sample with adsorbed CO_2 (CO_2-FAU) were studied at 4 K and at RT using the neutron diffraction technique. Modeling was also carried out to asset the geometry of the CO_2 molecules after they are adsorbed inside the zeolite.

2. Experimental[1]

2.1. Sample preparation

A 9.56 g sample of commercial sieve CBV-100 (zeolite NaY) was dried overnight in a tube furnace at 623 K in flowing nitrogen. The weight loss was 22.3%, corresponding to a composition of $Na_{56}Al_{56}Si_{136}O_{384}(H_2O)_{203}$.

A 6.953 g portion of the dried sieve was placed in a plastic jar with 2 cylindrical pieces of dry ice (12.7 mm diameter and 25.4 mm long), loosely capped. The sample was allowed to equilibrate for 8 h at 1 atmosphere (0.1 MPa) at the dry ice sublimation temperature (195 K). The weight gain was 1.823 g, corresponding to $Na_{56}Al_{56}Si_{136}O_{384}$ $(CO_2)_{76}$ (or a gain of 76 CO_2) if it is assumed that only CO_2 was adsorbed. Both the dehydrated (NaY) and CO_2-containing samples (NaY–CO_2) were placed inside a nitrogen-purged dry box, packed into 6 mm diameter vanadium cans, and sealed using indium gaskets, for the neutron diffraction studies.

2.2. Volumetric CO_2 sorption experiments

CO_2 sorption measurements were carried out at RT (298 K) in a computer controlled custom built Sieverts equipment previously described in detail [29], with an estimated reproducibility within 0.5% and isotherm data error bar of less than 2% compared to other commercial instruments [29]. Sample degassing, prior to CO_2 sorption experiment, was done at 623 K under vacuum for 20 h first, cool to room temperature and exposed to CO_2 up to about 1 atmosphere.

2.3. Neutron diffraction studies

Neutron diffraction studies were performed on the dehydrated NaY and the dehydrated sample with CO_2 (NaY–CO_2). The neutron diffraction experiments were carried out using 8 g of powder for each sample. Neutron diffraction data were collected with the 32 detector BT-1 diffractometer at the NIST Center for Neutron Research using a Cu(311) monochromator (λ = 1.5396(1) Å). Measurements were made under ambient conditions and at 4 K.

The structural refinements were performed using the GSAS software suite [30–31]. The framework structure of the NaY zeolite from literature [32] was employed as the initial model for refinements: NaY without CO_2 and with the incorporation of CO_2 under both ambient conditions and at 4 K. The neutron scattering lengths of the elements Na/Si/Al/C/O are 0.363/0.415/0.344/0.665/ 0.581×10^{-12} cm, respectively.

For dehydrated NaY, Rietveld refinement was begun with the (fixed) framework structure [32], and a difference Fourier map was calculated. The map indicated significant scattering densities at reasonable Na cation sites I, I′, and II, and these were added to the model as Na. No restraints were applied to bond distances or angles during the refinements. The refinement included atomic coordinates (Si and Al constrained), the lattice parameter, profile #2 coefficients *U, V, W, Y,* and *asym*, as well as a 12-term shifted Chebyshev background function [30–31]. A common *U* was refined for the framework oxygen atoms, and another common displacement parameter for the Na cations.

For NaY–CO_2, Rietveld refinement was initiated using the dehydrated NaY structure, and a difference Fourier map was calculated. Significant "blobs" of scattering density were added to the model as carbon atoms one at a time (with refining coordinates and occupancy but fixed *U*) until the difference Fourier map was judged to be acceptably flat. Extensive visualization and study of the extraframework atoms led to a chemically-reasonable and self-consistent identification of the adsorbed CO_2 molecules. A similar process was first applied to the RT diffraction pattern and then to the 4 K data sets. While in both cases a chemically-reasonable model was obtained, the RT data set ultimately did not yield residuals as good as the structure at 4 K.

During the refinement, the first CO_2 molecule, O12–C11–O13, was described as a rigid body with linear configuration. The residuals of refinements were not very sensitive to the position of this molecule. The O12–C11–O13 molecule was constrained to lie on a mirror plane (its true disorder may be more extensive). Although other interpretations of the scattering density in the supercage may be possible, this model yields the lowest residuals, and is chemically reasonable. The second CO_2 molecule, O16–C15–O16, was initially refined as a rigid body, but considerably better residuals were obtained by allowing the molecule to bend, using a combination of bonded (C═O, 1.18(1) Å) and non-bonded distance (O…O = 2.36(2) Å) restraints. Restraints were also applied to the T–O distances (1.63(2) Å), the O–T–O (T═Si/Al) angles (109(3)°), as well as the Na10–O12 distance (2.21(5) Å). A 3-term diffuse scattering function to describe an amorphous component was included in addition to the cosine Fourier series function.

After including the two CO_2 molecules in the model, additional electron density was found at the center of the sodalite cage, which was assigned as the oxygen of a water molecule (O19). Presumably a small amount of water was adsorbed by the zeolite during the exchange process. For the 4 K data set, an additional partially-occu-

[1] The purpose of identifying the equipment in this article is to specify the experimental procedure. Such identification does not imply recommendation or endorsement by the National Institute of Standards and Technology.

pied cation site (II′) in the sodalite cage was also included in the refinement as Na20.

3. Computational methods

Structural and total energy calculations were performed using the Vienna *ab initio* Simulation Package (VASP) [33] code based on self-consistent density functional theory (DFT). We used projector-augmented wave pseudopotentials [34–35] in conjunction with a plane wave expansion of the wave functions with a 300 eV cutoff energy. The spin-dependent generalized gradient approximation (GGA) with PBEsol (Perdew-Burke-Ernzerhof revised for solids) parameterization [36] was used to approximate the exchange and correlation functional. A 2x2x2 Monkhorst-Pack grid was applied to sample the Brillouin zone. Atomic positions and lattice vectors were fully relaxed. Force convergence was 0.01 eV/Å and energy 10 meV/unit cell.

4. Results and discussion

Before discussing in detail the structure of NaY with the presence of CO_2 molecules, it is important to first discuss the general structure of NaY. The NaY structure belongs to the well known faujasite crystal structure type (International Zeolite Association structure type FAU) [37]. Faujasite crystallizes in the cubic space group *Fd3m*, with a lattice constant ranging from 24.2 Å to 25.1 Å depending on the framework Al/Si concentration, types and concentration of the cations, and state of hydration [32]. The zeolite NaY can be visualized as being formed from 24-tetrahedra cuboctahedral units (sodalite cages), joined through hexagonal prisms (double 6-rings). There are a total of 192 tetrahedral Si/Al sites per unit cell. The structure of NaY can be viewed as the diamond structure, with the sodalite playing the role of carbon atoms, and the hexagonal prisms the role of C–C bonds. The pore structure is characterized by supercages approximately 12 Å in diameter, cavities which are linked through 12-ring windows about 8 Å in diameter.

Fig. 1 is the schematic diagram of the faujasite structure, illustrating the standard nomenclature for the framework atoms and the extraframework Na cation sites [38–40]. Na cations are commonly found in both the supercages and the sodalite cages. Several extraframework sites are commonly populated in cation-exchanged faujasites [38–40]. Several of these sites that were found to be occupied by Na in this study are listed below:

- I in the center of the hexagonal prism (double 6-rings).
- I′ in the sodalite cage, adjacent to a 6-ring shared by the sodalite cage and a double 6 ring.
- II in the supercage, adjacent to an unshared hexagonal face.
- II′ in the sodalite cage, adjacent to an unshared hexagonal face.
- II* in the supercage, toward the center from site II.
- U in the center of the sodalite cage.

The refinement results, including the final neutron refinement residuals, R_{wp}, R_p, goodness of fit (χ^2), R(F) and R(F)^2 are listed in Table 1. Figs. 2a–c give the Rietveld refinement plots for NaY, NaY–CO_2 at 4 K and NaY–CO_2 at RT, respectively. In these diagrams, the upper graph shows the fit between the experimental and calculated patterns while the lower graph shows the difference between these two patterns. Table 2 gives the lattice parameters,

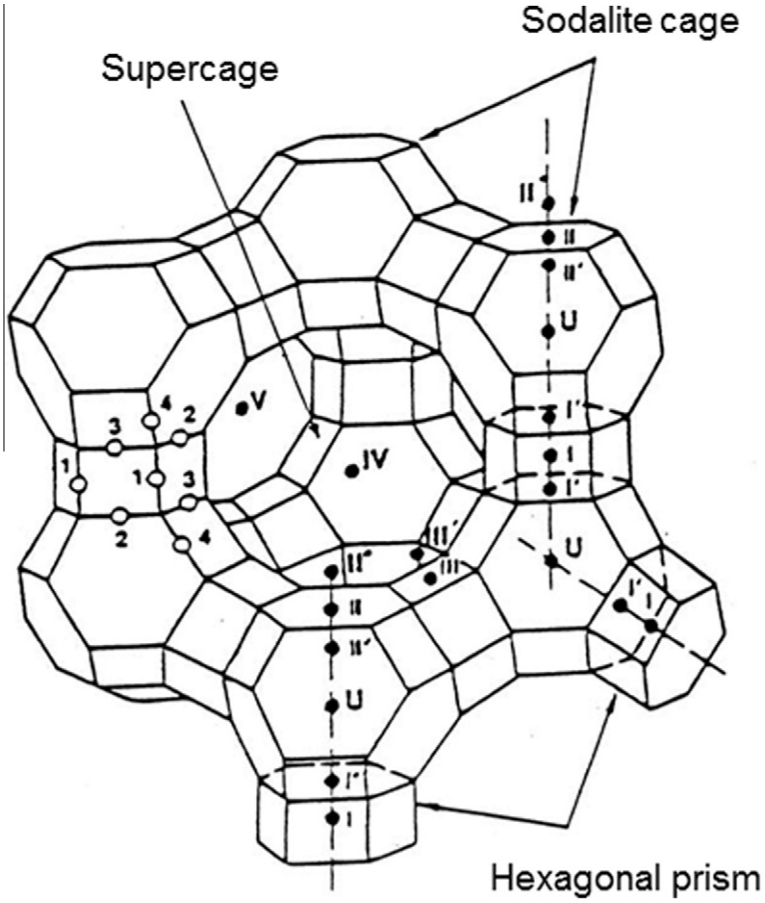

Fig. 1. The schematic diagram of the faujasite structure, illustrating the standard nomenclature for the framework atoms and the extraframework Na cation sites [38–40].

Table 1
Refinement Residuals for dehydrated NaY, NaY–CO_2 at ambient and 4 K.

State	Dehydrated	NaY–CO_2	NaY–CO_2
Temperature	Ambient	Ambient	4 K
R_{wp}	0.0567	0.0495	0.0428
R_p	0.0473	0.0397	0.0354
χ_2	1.055	1.203	1.812
$R(F)$	0.0381	0.0461	0.0450
$R(F)_2$	0.0491	0.0509	0.0690
ΔF, +	0.024	0.034	0.040
ΔF, −	−0.035	−0.032	−0.039

atomic coordinates, and isotropic displacement factors. Table 3 provides the cation-oxygen bond distances.

The atomic valences, V_b (obtained from bond valence sum (BVS) values), for the Na ions were calculated using the Brown–Altermatt empirical expression [41,42], and the results are also listed in Table 3. The V_b of an atom i is defined as the sum of the bond valences v_{ij} of all the bonds from atoms i to atoms j. The most commonly adopted empirical expression for the bond valence v_{ij} as a function of the interatomic distance d_{ij} is $v_{ij} = \exp[(R_0 - d_{ij})/B]$. The parameter, B, is commonly taken to be a "universal" constant equal to 0.37 Å. The value of the reference distance R_0 for Na–O is 1.80 [41,42]. One can in general consider the BVS as an indication for the strain state of the cations in a cage. A value that is larger than the ideal valence is considered to indicate compressive strain or overbonding, or the cage in which the cation resides is too small. On the other hand, a value smaller than the ideal value suggests tensile strain or coordinative unsaturation, or the cage is too large.

Results of the sorption experiments are shown in Fig. 3. The sorption curve illustrates the characteristics of a Type I isotherm. There is an increase of CO_2 adsorption at low equilibrium pressures and approach a plateau at 6.45 mmol/g. From this curve, our

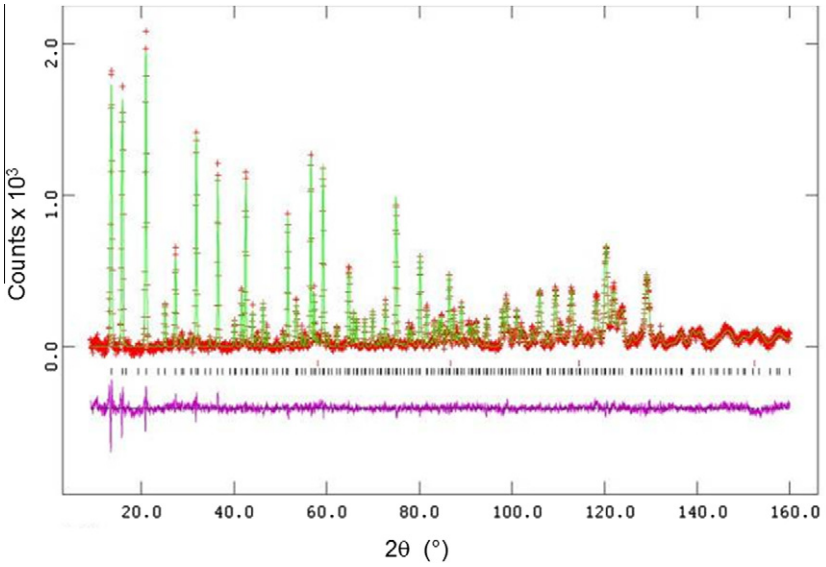

Fig. 2a. Rietveld refinement plots for dehydrated NaY at RT. In these diagrams, the upper graph shows the fit between the experimental and calculated patterns while the lower graph shows the difference between these two patterns.

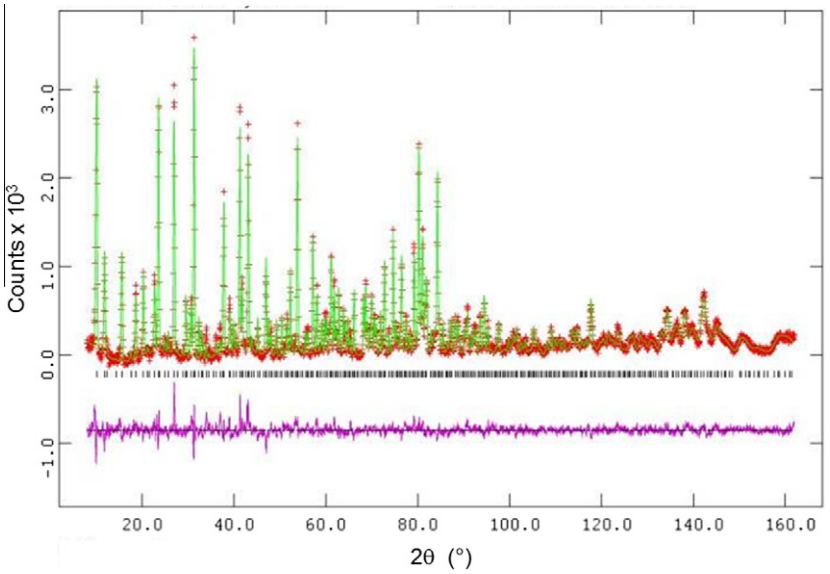

Fig. 2b. Rietveld refinement plots for dehydrated NaY in the presence of CO_2 at 4 K. In these diagrams, the upper graph shows the fit between the experimental and calculated patterns while the lower graph shows the difference between these two patterns.

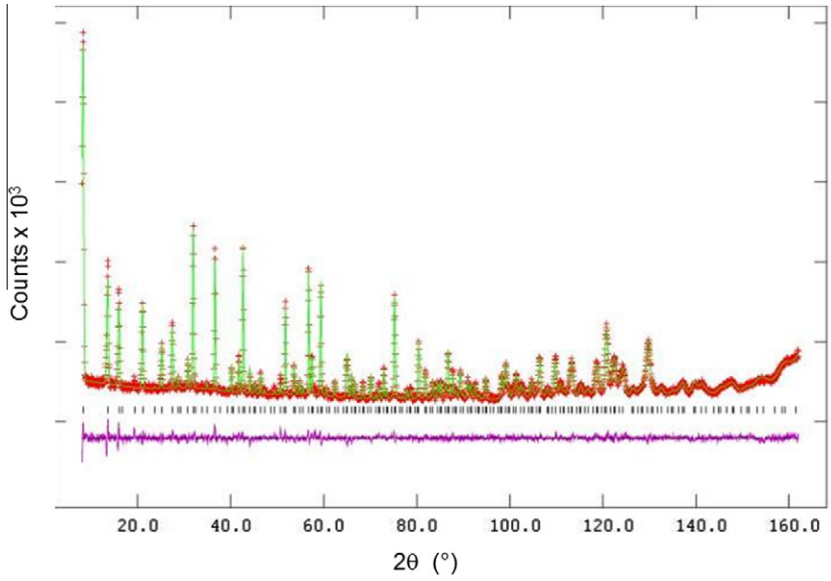

Fig. 2c. Rietveld refinement plots for dehydrated NaY in the presence of CO_2 at RT, respectively. In these diagrams, the upper graph shows the fit between the experimental and calculated patterns while the lower graph shows the difference between these two patterns.

sample is estimated to have a CO_2 content of about 6.0 mmol/g, corresponding to a weight gain of 76 CO_2.

In the following the structure description for NaY–CO_2 at 4 K will be described in detail. The structure of NaY–CO_2 at RT will be briefly compared to that at 4 K towards the end.

4.1. Structure of dehydrated NaY at RT

The structural literature on dehydrated NaY is extensive [32,40,43–48]. Cation locations in this material have been determined and reported at temperatures from 373 K to 996 K. Sites I, I′, and II are at all times occupied by Na. Occasionally traces of Na have been observed at sites II′ and U as well. For example, one specific literature study of the structure of dehydrated NaY at 20 K found 16 Na/cell at site I, 10 Na/cell at site II′, and 23 Na/cell at site II. Cation site populations are known to be influenced by the details of the drying process.

The composition of the dehydrated NaY used in this study was determined to be $Na_{56}Al_{56}Si_{138}O_{384}$. The weight loss on drying at 623 K corresponds to a typical water content of 203 H_2O/cell. The atomic coordinates of dehydrated NaY is given in Table 2. At RT, Na only occupies the I, II, and I' positions, but sites II′ and U were empty. All these sites lie on the 3-fold axis (*xxx*) on the body diagonal of the unit cell. Under ambient condition, 51 Na cations among a total of 56 were located. Cation positions I and I′ are too close to each other (about 2.6 Å) for both sites to be simultaneously occupied by Na. The sum of the (unconstrained) occupancy of these two sites was, however, found to be close to unity. Therefore the structure result represents a normal dehydrated NaY. As shown below, this framework will be used to compare with the NaY-CO_2 structure with adsorbed CO_2. Cation–cation repulsions play an important role as determining cation distribution. Not all Na can be accounted for by the occupation of these sites. The remaining Na is presumably disordered over sites in the supercage.

There are three crystallographically independent Na ions in the structure. Na7 (II), Na8 (I) and Na9 (I′) are found to be in the supercage, in the hexagonal prism and in the sodalite cage, respectively. The atomic valences of these cations (Table 3) indicated that they are coordinated to the framework oxygen atoms. The BVS value for Na8 is relatively small (0.56) as compared to the values of 0.82 and 0.94 for those for Na7 and Na9, indicating higher degree of tensile stress or underbonding.

4.2. Structure of dehydrated NaY with the adsorption of CO_2 (NaY–CO_2)

4.2.1. Structure at 4 K

The 4 K structure represents a snapshot of the 'frozen' CO_2 capture in the cages of dehydrated NaY under 0.1 MPa at the dry ice sublimation temperature. The framework structure of NaY was found to be essentially the same as that of the dehydrated NaY. The only difference is that some Na cations have been displaced as a result of interactions with CO_2. The binding arrangement that we have chosen to model the nuclear density accounts for the major peaks in the Fourier maps and generates chemically reasonable binding environments for the CO_2 molecules.

4.2.1.1. CO_2 in the supercage. Fig. 4 gives the structure of NaY–CO_2 at 4 K. The framework consists of corner-sharing TO_4 tetrahedra and the extraframework Na cations. There appears to be two different types of CO_2 molecules, with bent and linear configurations. In the linear CO_2 molecule, O12–C11–O13, the terminal O12 is coordinated to Na10, with the Na...O12–C11 angle of 135(2)°. As the coordination distance between them is relatively short (2.20(2) Å), there appears to be a relatively strong between the linear CO_2 molecule and Na10.

The bent CO_2 molecules O16–C15–O16 (148.3(3)°) were found to have a close distance from O16 to Na10 (on a 3-fold axis) of 2.836 (11) Å. As the CO_2 molecule is bent, we also investigated the possible carbonate formation as a result of the adsorption. As described by Bonenfant et al. [49], the formation of a stable monodentate carbonate species is possible via a three-step process. This will lead to the rupture of the Al–O bond and the oxygen will then be available to bond to C of the CO_2 group to form the carbonate. Adsorption of CO_2 in zeolites has been reported to be a result of dominant adsorption via interaction of the quadrupole moment of CO_2 and polar surface sites [50,51]. For example, Angell et al. [50] studied the behavior of CO_2 adsorbed on zeolites containing alkaline-earth cations and showed that the shift of the asymmetric stretching band can be correlated with the electrostatic field

Table 2
Crystal Structure (cell parameters, atomic coordinates, and displacement parameters of NaY (space group *Fd3m* (No. 227, origin choice # 2)).

	Dehydrated	With CO_2	With CO_2
Temperature	Ambient	Ambient	4 K
a, Å	24.7862 (2)	24.7342(2)	24.7288(2)
Si1/Al2, *x*	−0.0362(2)	−0.03565(14)	−0.03629(14)
y	−0.1239(2)	−0.12396(13)	−0.12382(12)
z	0.0545(2)	0.05407(12)	0.05420(11)
frac	0.71/0.29	0.71/0.29	0.71/0.29
Uiso, Å^2	0.0104(8)	0.0097(8)	0.0055(5)
O3, *x*	0	0	0
y	−0.1069(1)	−0.10758(13)	−0.10686(12)
Z	−0.1068(1)	0.10747(13)	0.10675(12)
Uiso (Å^2)	0.0284(5)	0.0272(5)	0.0152(4)
O4, *x*	0.0029(1)	0.00321(12)	0.00287(10)
y	−0.1423(2)	−0.14328(18)	−0.14348(17)
z	0.0029(1)	0.00321(12)	0.00287(10)
O5, *x*	−0.0724(1)	−0.07140(13)	−0.07255(11)
y	−0.0724(1)	−0.07140(13)	−0.07255(11)
z	0.0341(2)	0.03322(17)	0.03215(15)
O6, *x*	−0.0727(2)	−0.07419(15)	−0.07375(14)
y	−0.1774(2)	−0.17591(15)	−0.17365(14)
z	0.0674(2)	0.06792(18)	0.06860(16)
Na7 (II), *x,x,x*	0.2336(4)	0.23721(30)	0.23762(27)
Frac	0.85(3)	0.79(2)	0.77(2)
Uiso, Å^2	0.048(5)	0.0176(33)	0.0095(24)
Na/cell	27	25	25
Na8, (I), 0,0,0			
frac	0.60(3)	0.52(3)	0.25(3)
Na/cell	10	8	4
Na9 (I'), *x,x,x*	0.0545(7)	0.0618(13)	0.06421(52)
frac	0.45(3)	0.17(2)	0.36(2)
Na/cell	14	5	11
Na10 (II*), *x,x,x*		0.2827(11)	0.28598(77)
frac		0.22(2)	0.23(2)
Na/cell		7	7
Na20 (II'), *x,x,x*		–	0.21069(84)
frac			0.24(2)
Na/cell			8
O19, *1/8,1/8,1/8*			
frac		1.08(7)	1
C11, *x*		0.3987(23)	0.3987(7)
y		0.2541(13)	0.2444(6)
z		0.2541(13)	0.2444(6)
Frac		0.217(9)	0.200(7)
Uiso, Å$_2$		0.504(22)	0.145(6)
O12, *x*		0.3719(42)	0.3728(10)
y		0.2820(29)	0.2728(9)
z		0.2820(29)	0.2728(9)
O13, *x*		0.4256(27)	0.4245(12)
y		0.2262(29)	0.2161(11)
z		0.2262(29)	0.2161(11)
C15, *x*		0.2074(23)	0.1895(9)
y		3/8	3/8
z		3/8	3/8
Frac		0.49(2)	0.546(11)
Uiso, Å2		0.504(22)	0.145(6)
O16, *x*		0.2128(20)	0.2028(7)
y		0.4086(2)	0.4082(2)
z		0.4086(2)	0.4082(2)

Table 3
Cation–Oxygen Bond Distances (Å) in dehydrated NaY, NaY–CO_2 at ambient and 4 K.

State	Dehydrated NaY	NaY–CO_2	NaY–CO_2
Temperature	Ambient	Ambient	4 K
Na7–O4 × 3	2.361(7)	2.390(6)	2.388(6)
Na7–O6 × 3	2.869(6)	2.931(6)	2.934(5)
BVS(II)	0.82	0.75	0.75
Na8–O5 × 6	2.674(5)	2.629(5)	2.659(4)
BVS(I)	0.56	0.64	0.59
Na9–O3 × 3	2.963(6)	3.039(14)	3.057(7)
Na9–O5 × 3	2.284(11)	2.375(26)	2.401(11)
Na9–O19	–	2.71(6)	2.604(22)
BVS(I')	0.94	0.82	0.80
Na10–O12 × 3		2.21(11)	2.20(2)
Na10–O16 × 3		2.682(31)	2.836(11)
BVS		1.27	1.21
Na20–O4 × 3		–	2.222(5)
Na20–O6 × 3			2.927(8)
BVS			1.10

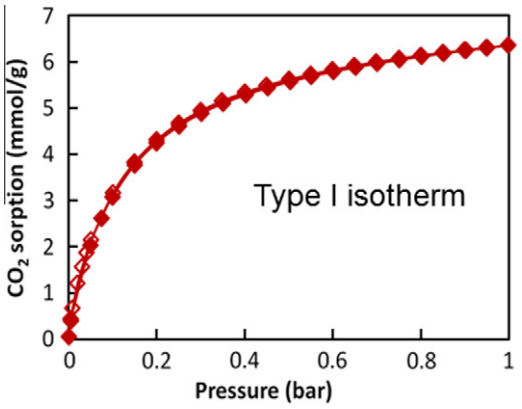

Fig. 3. The CO_2 sorption isotherm of NaY at 298 K showing the Type I isotherm feature. The filled diamonds correspond to adsorption curve and the empty diamonds correspond to the desorption curve. An increase of CO2 adsorption at low equilibrium pressures which approaches a plateau at 6.45 mmol/g is shown.

strength due to the cations. Ward and Habgood [51] found stretching bands that were ascribed to CO_2 chemisorbed on surface oxygen to give a bent carbonate-like structure. In our case, judging from the atomic distances of C15 to O3, O4, O5, and O6, the formation of the C–O bond with framework oxygen from the Al–O group did not occur. None of these distances can be considered as a C–O bond as they are all greater than 3 Å. Furthermore, the Na10–O16–C15 bond angle was found to be rather large, at 149.3(10)°. These observations indicate that neither the unidentate carbonate nor bidendate carbonate formed [50] as a result of the interaction.

The presence of the bent CO_2 groups could be a result of two possibilities. In the first, the weak interaction of oxygen atoms at both ends of the CO_2 molecule with Na10 leads to a bridging Na–O16–C15–O16–Na unit, instead of carbonate groups with expected O–C–O angle of approximately 120°. It is possible that formation of this type of extended coordination will eventually prevent the further diffusion of CO_2 into the supercage. Another possible explanation of the bent CO_2 molecule is disorder. The bending appearance could be due to two linear rotationally disordered CO_2 molecules (both with partial occupancy). The adsorbed CO_2 molecule is attached to Na through one of is oxygen atoms while the rest of the molecule is free to rotate, resulting in a circular trajectory for the second oxygen atom (Fig. 5). Because of the rotational disorder, the nuclear density of the second oxygen atom is too low to locate. The difference Fourier map is essentially flat in the pertinent regions. The 'overlap' with another disorder CO_2 (also with partial occupancy) unit generated by *mm* site symmetry will give rise to an average structure of a bent molecule. Yildirim and co-workers [52] also observed bent CO_2 molecules in the MOF 74 system due to rotational disorder.

Results of DFT total energy calculations suggested that the van der Waals interaction did not play a crucial role in the interaction of Na10 and CO_2, which was dominated by the electrostatic interaction. The potential energy curve was estimated as a function of

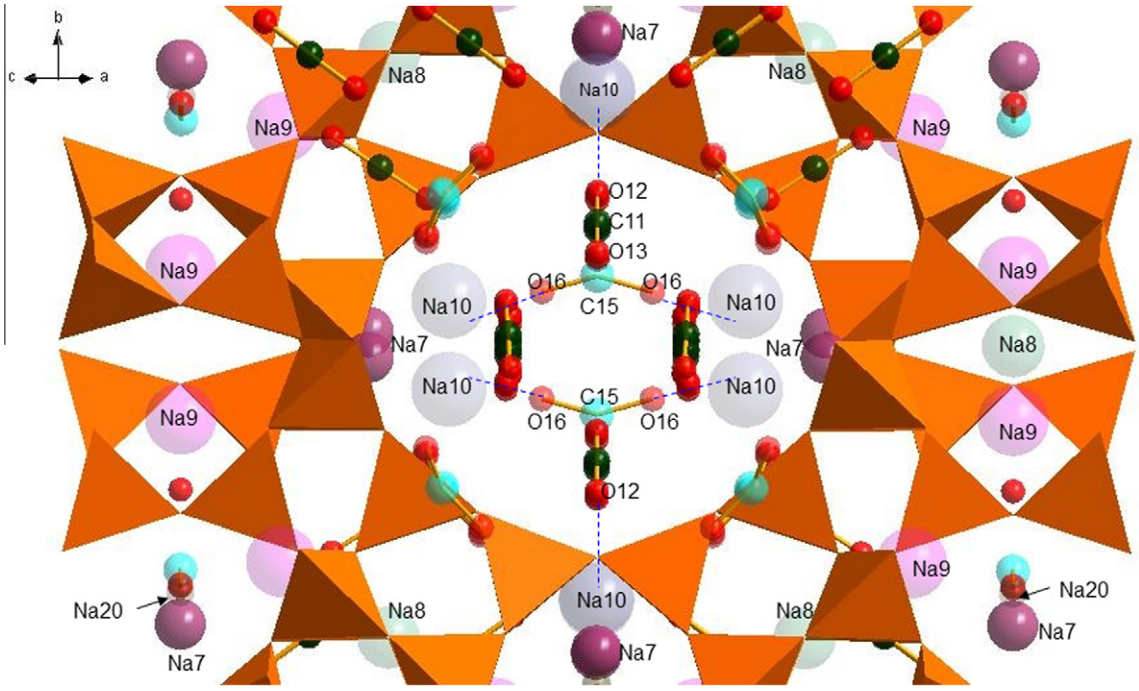

Fig. 4. Structure of NaY-CO_2 at 4 K. The framework consists of corner-sharing TO_4 tetrahedra and the extraframework Na cations. Two different configurations of CO_2 molecules (linear and bent) are found inside the supercage.

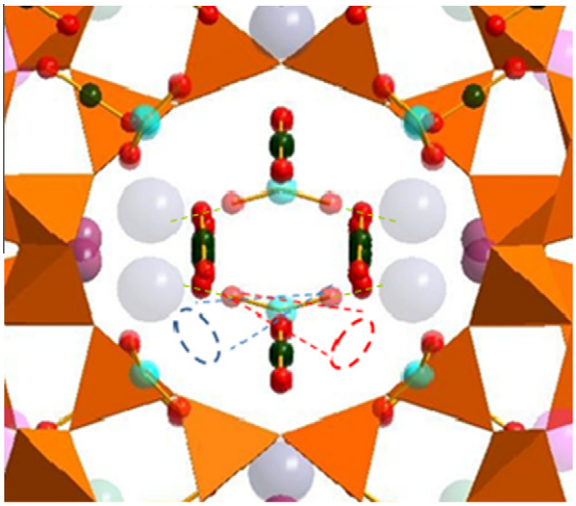

Fig. 5. Schematic representation of the rotational disorder of two CO_2 molecules (along the Na–O axis) resulting in a circular trajectory for the second O atom.

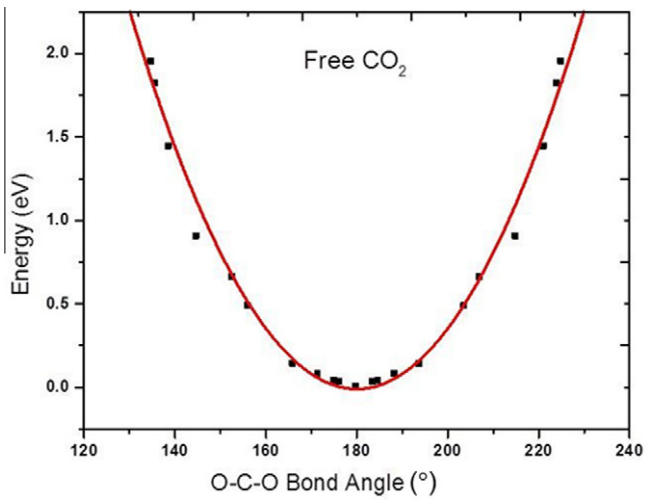

Fig. 6. Energy cost of the O–C–O bending motion for a free CO_2 molecule, estimated by DFT calculations.

O–C–O bond angle for a free CO_2 molecule. In Fig. 6, the 32° bond angle distortion in free CO_2 costs a significant energy of ≈0.66 eV/CO_2. We placed the CO_2 molecule with the bond angle of 148.3° in the crystal structure of dehydrated NaY with cell parameters and atomic coordinates derived from experiments (Table 2). Cell and atomic positions were fully relaxed, except CO_2 molecules with the fixed O–C–O angles of 148°, followed by a high-precision total energy calculation. The interaction of Na10 and CO_2 can facilitate the bending motion for CO_2 by decreasing the energy cost for the 148.3° angle by ≈0.2 eV/CO_2, which is not sufficient to cause the 32° bond angle distortion. Therefore, it is still possible that the CO_2 adopts a small bent configuration (Fig. 6), but rotational disorder appears to play an important role leading to the observed large bending angle.

4.2.1.2. Migration of extraframework Na cations. Adsorption of CO_2 results in a migration and rearrangement of the extraframework Na cations and a complex network of interactions between the adsorbed CO_2 molecules and Na cations in the supercages (Fig. 7). At 4 K, nearly all of the Na cations were located. The Na II (Na7) site is mostly occupied (about 80%). A comparison of the current structure to the structure of dehydrated NaY shows that as a result of interaction with adsorbate CO_2 molecules (Table 1 and Fig. 4), movement of about 20% of Na7 (II) by 2.07 Å into site II* (becoming Na10) of the supercage was observed. This movement opens space, and apparently site II′ inside the sodalite cage is also occupied by a Na ion when the coordinated Na is presented at the II* site. In summary, Na10 is coordinated to three O12 atoms and three O16 atoms of the CO_2 molecules (all with partial occupancy). In Fig 4,

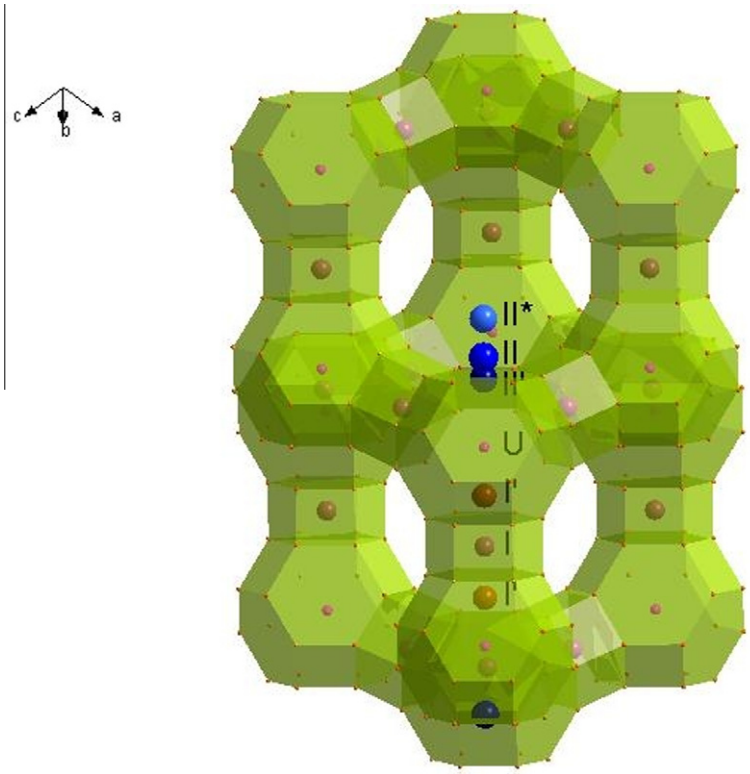

Fig. 7. Adsorption of CO_2 results in a migration and rearrangement of the extraframework Na cations. A portion of the Na7 (II) is migrated into site II* (Na10) of the supercage was observed. This movement opens space, and apparently site II′ inside the sodalite cage is also occupied by a Na when the coordinated Na is present at the II* site.

a few representative CO_2 groups that involve Na10. . .O16 as well as Na10. . .O12 are shown.

In addition to the presence of Na10 in the supercage, a further partially-occupied cation site (II′) was also included as Na20. This II′ site, as described earlier, lies in the sodalite cage, adjacent to an unshared hexagonal face. Na20 is associated with O(4) with a distance of 2.222(5) Å and O(6) with a distance of 2.927(8) Å, respectively. As a result of the interactions between various Na cations and CO_2, the distances between Na7–O (II-supercage) and Na9–O (I′-sodalite cage) are longer than the corresponding distance in NaY without CO_2, while the distance between Na8–O5 (I- center of the hexagonal prism) is shorter.

The migration of extraframework cations during adsorption and desorption process of zeolites has been studied by Beauvais et al. [53] and Pichon et al. [54] with water molecules. They observed water migrate to a variety of sites. Plant et al. [55–57] modeled the diffusion of CO_2 in the Faujasite systems using molecular dynamics simulations which were directly compared to their quasielastic neutron scattering measurements [55,56]. They were able to determine the cation motion upon adsorption of CO_2 from their spectroscopic and modeling studies. They found that at low and intermediate loading of CO_2, the Na II cations can migrate towards the center of the supercage. Our diffraction data provides direct evidence of this type of cation migration.

4.2.1.3. Presence of water molecules in NaY–CO_2. In addition to the presence of the CO_2 molecules in the model, in the center of the sodalite cage density attributed to the oxygen (O19) of a water molecule was also observed. Water molecules were not located in the supercage. O19 was found to associate with Na9 (I′) which also lies in the sodalite cage and is adjacent to a 6-ring shared by the sodalite cage and a hexagonal prism.

Apparently there is selectivity for the gas molecule concerning which cage to enter during the adsorption process of NaY. The principal factors influencing carbon dioxide adsorption on zeolites have been summarized by Bonenfant et al [49]. These factors include structural characteristics of the host (basicity, polarizing power, distribution, size and number of exchangeable cations, influence of the Si/Al ratio, influence of the size of pores), as well as influence of adsorbate characteristics (polarity, molecular dimensions, carbonate formation, presence of water, prevailing pressure and temperature). The pore size of zeolite is another factor that influences the capacity and rate of CO_2/gas adsorption. Because the H_2O molecule is smaller than CO_2, it is expected to primarily occupy the relatively smaller sodalite cage.

4.2.1.4. Atomic valence of extraframework Na cations (V_b). The V_b values for the five crystallographically independent Na ions in the structure are shown in Table 3. In addition to Na7 in the supercage, Na8 in the hexagonal prism and Na9 in the sodalite cage, Na10 is found in the supercage with a 0.23 occupancy and Na20 is in the solidate cage with a 0.24 occupancy. Similar to the dehydrated NaY, while the V_b values for Na7, Na8 and Na9 are all smaller than the ideal value of '1', the value for Na8 is particularly small (0.59 as compared to the values of 0.75 and 0.80 for those associated with Na7 and Na9), indicating higher degree of underbonding or weak bonding. On the other hand, the bonding environment for Na10 and Na20 is rather different as their V_b values are greater than 1.0, indicating somewhat compressive stress or overbonding.

4.2.1.5. Stoichiometry of NaY determined at 4 K. At 4 K, the refined composition of NaY is $Na_{48}Al_{56}Si_{136}O_{384}(CO_2)_{45}(H_2O)_8$. This formula corresponds to a 17% weight gain, compared to the observed 26% weight gain. Assuming this gain is due to only CO_2 adsorption, this result corresponds to 76 CO_2/cell. Our refinement results

indicate the occupancy of the linear CO_2 sites to be about 20%, the "bent" CO_2 sites to be of 55% and the absorbed H_2O molecule in the sodalite site to be of 100% (or 8 H_2O molecules per unit cell). Apparently not all of the adsorbed material is localized, as there is difference between weight loss and the refinement result. It is probable that more CO_2 molecules and water molecules were adsorbed during exposure. Water is known to have a high tendency to be disordered in broad channels as well. However, due to their highly disordered structure, they were not located.

4.2.2. Structure of NaY–CO_2 at RT

A comparison of the NaY–CO_2 structure at RT and at 4 K indicates that in general the structures are similar except for the angle of O16–C15–O16 of the CO_2 molecule (Tables 1 and 2). For example, the occupancy values of both crystallographically independent CO_2 sites (0.217(9) (RT) vs 0.200(7) (4 K)) and (0.49(2) (RT) vs 0.546(11) (4 K)) are comparable. The angles of Na10–O16–C15 (146(4)°) and Na10–O12–C11 (125(8)°) are also comparable to those found in the 4 K data. At RT, the displacement coefficients are larger for all atoms and fewer Na atoms could be located (also due to extensive disorder) as compared to the structure determined at 4 K. For example, instead of 11 Na9 in the supercage, only 8 were located at RT. Na20 which is observed at 4 K in the sodalite cage, is absent at RT.

Similar to the 4 K structure, the two possible explanations for the observed bent angle for CO_2 are the rotational disorder and a result of the double bridging to Na10 on both sides of the CO_2 molecule. The 167(7)° bending angle of O16–C15–O16 is substantially greater than the corresponding 148.3(3)° found in the 4 K structure. At a first glance from Fig. 6, the 13° bond angle distortion in free CO_2 costs the energy of ≈0.14 eV/CO_2, which can likely be reduced via the interaction of Na10 and CO_2. However, as the 4 K structure suggested that rotational disorder appears to play an important role leading to the observed large bending angle, it is logical that at room temperature rotational disorder plays an even bigger role to the observed bent structure.

Our refinement results also indicate that the occupancy for the absorbed H_2O (O19) molecule in the sodalite cage is 100% at RT and at 4 K (8 H_2O molecules per unit cell). This H_2O molecule is weakly bonded to Na9 with a distance of 2.71(6) Å.

At RT, there are only four crystallographically independent Na ions in the structure. A comparison with the structure of NaY–CO_2 at 4 K indicates that Na20 is not found at RT, but Na10 appears in the supercage with a comparable 0.22(2) occupancy. The BVS values (Table 3) for Na7, Na8 and Na9 are similar to those for the 4 K data as well. Na10 exhibits compressive stress or overbonding situation.

5. Conclusions and future work

The structure of dehydrated NaY is comparable to that obtained from previously reported diffraction studies. The framework structure of dehydrated NaY and that of dehydrated NaY with adsorbed CO_2 are quite similar except for the locations of Na cations. The appreciably different structures of NaY–CO_2 at RT and at 4 K are mostly attributed to the fact that the structure at RT has a higher degree of disorder for Na ions and CO_2. This study also demonstrates that cation occupancies and positions are different at RT and at 4 K, therefore cation distribution cannot be assumed, but must be determined at the temperature of interest. Cation–cation repulsions play an important role as determining the cation distribution.

Most of the CO_2 molecules as estimated from weight gain of samples before and after the CO_2 adsorption experiments were located using neutron diffraction experiments. Adsorption of CO_2 results in a migration and rearrangement of the extraframework Na cations and a complex network of interactions between the adsorbed CO_2 molecules and Na cations in the supercages. Two different configurations of CO_2 were located, linear and bent. The linear CO_2 molecule coordinates with 20% of the Na7 site via the oxygen sites while the seemingly bent molecules that also interact with Na7 is a consequence of rotational disorder. As a result of these complex interactions, 20% of Na7 migrated from the unshared hexagonal cage to the new Na site (Na10) towards the center of the supercage. This movement opens space, and apparently site II′ inside the sodalite cage is also occupied by a Na ion when the coordinated Na is present at the II* site. As a result, each Na10 is coordinated to six partially occupied oxygen atoms from CO_2 molecules (three O12 and three O16).

Future work includes structure determination of NaY with CO_2 as a function of p_{CO2} so one can understand the CO_2 adsorption mechanism in more detail. It is also important to study other zeolites with different cage sizes to correlate the effect of cage volume and the locations of adsorbed CO_2.

Acknowledgement

The valuable scientific discussion with Dr. T. Yildirim of NIST Center for Neutron Research is acknowledged.

References

[1] Kenji Sumida, David L. Rogow, Jarad A. Mason, Thomas M. McDonald, Eric D. Bloch, Zoey R. Herm, Tae-Hyun Bae, Jeffrey R. Long, Chem. Rev. 112 (2012) 724–781.
[2] Jian Liu, Praveen K. Thallapally, B. Peter McGrail, Daryl R. Brown, Jun Liu, Chem. Soc. Rev. 41 (2012) 2308.
[3] Gérard Férey, Christian Serre, Thomas Devic, Guillaume Maurin, Hervé Jobic, Philip L. Llewellyn, Guy De Weireld, Alexandre Vimont, Marco Daturi, Jong-San Chang, Chem. Soc. Rev. 40 (2011) 550.
[4] Youn-Sang Bae, Randall.Q. Snurr, Angew. Chem. Int. Ed. 50 (2011) 11586–11596.
[5] Ramanathan Vaidhyanathan, Simon S. Iremonger, George K.H. Shimizu, Peter G. Boyd, Saman Alavi, Tom K. Woo, Science 330 (2010) 650.
[6] Wen-Yang Gao, Wuming Yan, Rong Cai, Kia Williams, Andrea Salas, Lukasz Wojtas, Xiaodong Shi, Shengqian Ma, Chem. Commun. 48 (2012) 8898–8900.
[7] Shengqian Ma, Hong-Cai Zhou, Chem. Commun. 46 (2010) 44–53.
[8] M. O'Keeffe, O.M. Yaghi, Chem. Rev. 112 (2012) 675–702.
[9] S. Choi, J.H. Drese, C.W. Jones, ChemSusChem 2 (9) (2009) 796–854.
[10] J.H. Chen, D.S.H. Wong, C.S. Tan, Ind. Eng. Chem. Res. 36 (7) (1997) 2808–2815.
[11] J.C. Hicks, J.H. Drese, D.J. Fauth, M.L. Gray, G. Qi, C.W. Jones, J. Am. Chem. Soc. 130 (10) (2008) 2902–2903.
[12] T. Sakakura, Y. Saito, M. Okano, J.-C. Choi, T. Sako, J. Org. Chem. 63 (20) (1998) 7095–7096.
[13] T. Ohsumi, Energ. Convers. Manage. 34 (9–11) (1993) 1059–1064.
[14] R.E. Morris, P.S. Wheatley, Angew. Chem. Int. Ed. 47 (27) (2008) 4966–4981.
[15] B.H. Toby, J. Res. Natl. Inst. Stand. Technol. 106 (6) (2001) 965–973.
[16] G.T. Kokotailo, C.A. Fyfe, Rigaku J. 12 (1) (1995) 3–10.
[17] J. Merel, M. Clausse, F. Meunier, Ind. Eng. Chem. Res. 47 (1) (2008) 209–215.
[18] M.T. Ho, G.W. Allinson, D.E. Wiley, Ind. Eng. Chem. Res. 47 (14) (2008) 4883–4890.
[19] M.R. Hudson, W.L. Queen, J.A. Mason, D.W. Fickel, R.F. Lobo, C.M. Brown, J. Am. Chem. Soc. 134 (4) (2012) 1970–1973.
[20] W. Shao, L. Zhang, L.X. Li, R.L. Lee, Adsorption 15 (5–6) (2009) 497–505.
[21] J.C. Santos, F.D. Magalhaes, A. Mendes, Ind. Eng. Chem. Res. 47 (16) (2008) 6197–6203.
[22] I. Deroche, L. Gaberova, G. Maurin, P. Llewellyn, M. Castro, P. Wright, Adsorption 14 (2/3) (2008) 207–213.
[23] G. Maurin, P.L. Llewellyn, R.G. Bell, J. Phys. Chem. B 109 (33) (2005) 16084–16091.
[24] E. Jaramillo, M. Chandross, J. Phys. Chem. B 108 (52) (2004) 20155–20159.
[25] R. Ghezini, M. Sassi, A. Benguedach, Microporous Mesoporous Mater. 113 (1–3) (2008) 370–377.
[26] D. Selassie, F. Amankona-Diawuo, D. Kohen, Abs. Papers, 235 ACS Nat. Meet. 2008.
[27] E. Diaz, E. Munoz, A. Vega, S. Ordonez, Chemosphere 70 (8) (2008) 1375–1382.
[28] D. Plant, H. Jobic, P. Llewellyn, G. Maurin, Eur. Phys. J. 141 (2007) 127–132.
[29] W. Zhou, H. Wu, M.R. Hartman, T. Yildirim, J. Phys. Chem. C 111 (2007) 16131–16137.
[30] H.M. Rietveld, J Appl. Cryst. 2 (1969) 65–71.
[31] A.C. Larson, R.B. von Dreele, "GSAS-General Structure Analysis System", US Government contract (W-7405-ENG-36) by the Los Alamos National

laboratory, which is operated by the University of California for the U.S. Department of, Energy, 1992.
[32] J.A. Kaduk, Crystallogr. Rev. 11 (1) (2005) 1–19.
[33] G. Kresse, J. Furthmuller, Phys. Rev. B 54 (1996) 11169.
[34] P.E. Blöchl, Phys. Rev. B 50 (1994) 17953.
[35] G. Kresse, D. Joubert, Phys. Rev. B 59 (1999) 1758.
[36] J.P. Perdew, A. Ruzsinszky, G.I. Csonka, O.A. Vydrov, G.E. Scuseria, L.A. Constantin, X. Zhou, K. Burke, Phys. Rev. Lett. 100 (2008) 136406.
[37] W.M. Meier, D.H. Olson, Atlas of Zeolite structure, 5th ed., Elsevier, Amsterdam, 2001. W.M..
[38] H. Klein, C. Kirschhock, H. Fuess, J. Phys. Chem. 98 (47) (1994) 12345–12360.
[39] J.V. Smith, Adv. Chem. Ser. 101 (1971) 171–200.
[40] W. J. Mortier, Compilation of Extra Framework Sites in Zeolites, Butterworth, London. (1982), 67.
[41] I.D. Brown, D. Altermatt, Acta Crystallogr. B41 (1985) 244–247.
[42] N.E. Brese, M. O'Keeffe, Acta Crystallogr. B47 (1991) 192.
[43] C.P. Grey, F.L. Poshni, F. Gualtieri, P. Norby, J.C. Hanson, D.R. Corbin, J. Am. Chem. Soc. 119 (1997) 1981.
[44] A.J. Fowkes, R.M. Ibberson, M.J. Rosseinsky, Chem. Mater. 14 (2002) 590–602. ICSD collection code 94779.
[45] P. Gallezot, B. Imelik, J. Chim. Phys. 68 (1971) 816–821. ICSD collection codes 33599–33601.
[46] J.A. Hriljac, M.M. Eddy, A.K. Cheetham, J.A. Donohue, G.J. Ray, J. Solid State Chem. 106 (1993) 66–72. ICSD collection code 73929.
[47] A.N. Fitch, H. Jobic, A. enouprez, J. Phys. Chem. 90 (1986) 1311–1318. ICSD collection code 40927.
[48] G.R. Eulenberger, D.P. Shoemaker, J.G. Keil, J. Phys. Chem. 71 (1967) 1812–1819. ICSD collection code 22278.
[49] D. Bonenfant, M. Kharoune, P. Niquette, M. Mimeault, R. Hausler, Sci. Technol. Adv. Mater. 9 (2008) 013007.
[50] C.L. Angell, M.V. Howell, Can. J. Chem. 47 (1969) 3831–3836.
[51] J.W. Ward, H.W. Habgood, J. Phys. Chem. 70 (4) (1966) 1178.
[52] H. Wu, J. Simmions, G. Srinivas, W. Zhou, T. Yildirim, J. Phy, Chem. Lett. 1 (2010) 1946–1951.
[53] C. Beauvais, A. Boutin, A.H. Fuchs, Chem. Phys. 3 (2004) 179.
[54] C. Pichon, H. Palancher, J. Lynch, J.L. Hordeau, J.F. Berar, in: Molecular Sieves: From Basic Research to Industrial Applications, in: J. Čejka, N. Žilková, P. Nachtigall, Proceedings of the 3 International Zeolite Symposium (3 FEZA), Prague, Czech Republic, 23–26 August 2005, Stud Surf Sci Catal A&B 158 (2005), 789, ISBN: 978-0-444- 51670-1.
[55] D.F. Plant, H. Jobic, P.L. Llewellyn, G. Maurin, Adsorption 13 (3–4) (2007) 209.
[56] D.F. Plant, H. Jobic, P.L. Llewellyn, G. Maurin, Adsorption 15 (5–6) (2009) 497.
[57] D.F. Plant, G. Maurin, H. Jobic, P.L. Llewellyn, J. Phys. Chem. B 110 (2006) 14372–14378.